Identification of Cr^{3+} centers in Cs_2NaAlF_6 and Cs_2NaGaF_6 crystals by EPR and ENDOR paramagnetic resonance techniques

H. Vrielinck, F. Loncke, F. Callens,* and P. Matthys
Ghent University, Department of Solid State Sciences, Krijgslaan 281 – S1, B-9000 Gent, Belgium

N. M. Khaidukov
Institute of General and Inorganic Chemistry, 31 Leninskii Prospect, 119991 Moscow, Russian Federation
(Received 3 May 2004; published 25 October 2004)

Chromium-doped Cs_2NaAlF_6 and Cs_2NaGaF_6 crystals have been investigated by using the techniques of electron paramagnetic resonance (EPR) and electron nuclear double resonance (ENDOR) at *X*-band (9.5 GHz) and *Q*-band (34 GHz) frequencies. In both crystals, which have the hexagonal elpasolite structure, two inequivalent Cr^{3+} centers are detected. From the angular dependence of the ENDOR spectra for the central ^{53}Cr nucleus and the nearest shells of ^{19}F and ^{23}Na nuclei, the crystallographic sites at which the paramagnetic Cr^{3+} ions are incorporated in these crystals have been unambiguously determined for each type of center. The results of the EPR and ENDOR investigation are discussed in the context of their correlation with optical and crystallographic data for these crystals and give considerable information about local distortions around the paramagnetic impurity ions.

DOI: 10.1103/PhysRevB.70.144111 PACS number(s): 76.30.Fc, 76.70.Dx, 42.55.Rz, 42.70.Hj

INTRODUCTION

In the past few years there has been considerable progress in developing various semiconductor diode lasers covering the spectral range from infrared to ultraviolet. Such lasers gradually replace other laser sources, in particular optically pumped solid-state lasers, in different fields of applications. However, at present semiconductor lasers are not able to compete with optically pumped solid-state lasers in the fields where laser sources with a high pulse repetition rate, ultrashort pulse duration and high peak intensity are required.[1] In this context, there is a certain success in developing compact diode-pumped femtosecond solid-state lasers based on fluoride crystals, having the colquiriite structure, doped with Cr^{3+}, in particular Cr^{3+}:$LiSrAlF_6$.[2,3] This stimulates developing new Cr^{3+} laser materials based on glasses, oxide and fluoride crystals having broader wavelength coverage, greater storage capacity, better quantum yield, higher stimulated cross section, and less excited-state absorption than Cr^{3+}:$LiSrAlF_6$.[4–6] Moreover, due to its specific energetic structure, Cr^{3+} is a very effective spectroscopic probe which allows determining dynamic and static properties of crystallographic sites for active ions in different hosts.[7–9]

From the viewpoint of basic research and prospects for applications, hexagonal elpasolites doped with Cr^{3+} are more attractive objects than some well studied cubic elpasolites, e.g., Cr^{3+}:K_2NaScF_6 (Ref. 10) and Cr^{3+}:$Cs_2NaScCl_6$.[8] Considerable experimental efforts have recently been paid for investigating hexagonal Cr^{3+}-doped Cs_2NaAlF_6 and Cs_2NaGaF_6 crystals with optical absorption and fluorescence spectroscopy,[11–13] x-ray and neutron diffraction,[14,15] Raman spectroscopy,[14,15] luminescent quantum efficiency measurements,[16] and electron paramagnetic resonance (EPR).[17,18]

In the hexagonal elpasolite lattice there are two inequivalent crystallographic sites for trivalent ions M^{3+},[19] as indicated in Fig. 1. Both sites have a sixfold nearly regular octahedral fluorine coordination, slightly distorted to D_{3d} symmetry along the *c* axis of the crystal, but differ considerably with respect to their nearest cation environment. For one of the sites, which is labeled as $M1$,[19] the MF_6 octahedron is connected to six NaF_6 octahedra via common corners, whereas the other, $M2$, is connected to only two NaF_6 polyhedra along the *c* axis through common faces. The position also has a sixfold fluorine coordination, but has local C_{3v} symmetry. The two inequivalent Cs^+ positions are twelvefold coordinated and also have local C_{3v} symmetry.

Using optical[11,12] and EPR spectroscopy,[17,18] it has been established that there are two inequivalent Cr^{3+} centers in Cr^{3+}:Cs_2NaAlF_6 and Cr^{3+}:Cs_2NaGaF_6 crystals, which has been attributed to Cr^{3+} ions substituting at the two inequivalent M^{3+} sites. Following the EPR results, each of these axially symmetric Cr^{3+} centers has been assigned to a particular crystallographic site considering the magnitude of its zero field splitting ($S=3/2$).[17,18] Indeed, one can expect from the crystallographic data[14,15] that the axial component of the crystal field at site $M1$ is smaller than at site $M2$. In both hosts the EPR zero field splitting for one of the Cr^{3+} centers, denoted as $C1$, is considerably smaller than that for the other, $C2$, so it seemed reasonable to identify the former as Cr^{3+} at site $M1$ and the latter as Cr^{3+} at site $M2$.[17,18] Furthermore, ^{53}Cr electron nuclear double resonance (ENDOR) measurements on Cr^{3+}:Cs_2NaGaF_6 powders have revealed that the zero field splitting parameters (D) for the two centers have opposite signs.[18] However, the EPR results do not exclude the possibility of Cr^{3+} substitution on the monovalent cation sites, which would also give rise to centers with axial symmetry. Except for cases where superhyperfine (shf) structure is resolved, EPR fails to make the distinction between centrosymmetric (M^{3+} positions with D_{3d} symmetry) and noncentrosymmetric complexes (Cs^+ and Na^+ positions with C_{3v} symmetry).[20,21] Moreover, if local lattice distortions due to the substitution need to be considered, it is not *a priori*

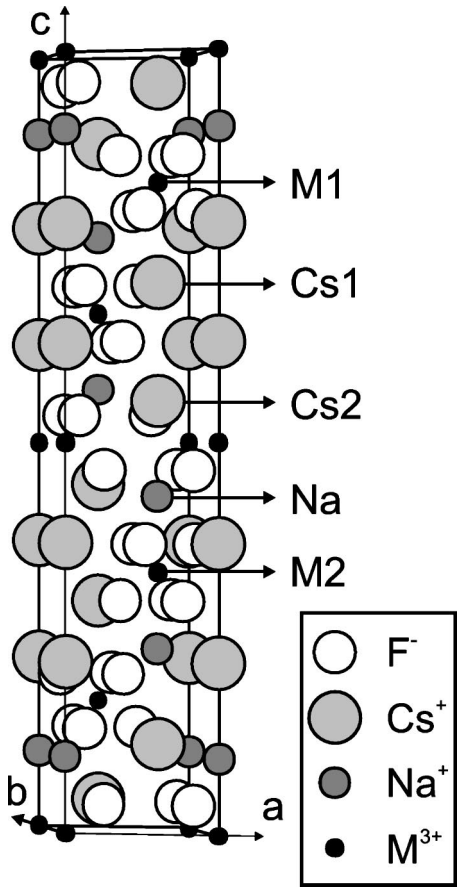

FIG. 1. Unit cell of the hexagonal elpasolite crystals Cs_2NaMF_6. The two inequivalent Cs^+ (Cs1, Cs2), the Na^+ (Na) and the two inequivalent M^{3+} ($M1$, $M2$) positions in the lattice are indicated.

obvious that the EPR argument for the Cr^{3+} center assignations still holds.

The Cr^{3+} center assignations from optical spectroscopy are primarily based on measurements of the fluorescence lifetime, which is expected to decrease if the deviation from cubic symmetry becomes larger. Therefore, in both crystals the center with the longer lifetime has been identified as Cr^{3+} at site $M1$ where the octahedral symmetry is less distorted.[11,12] The splitting of the zero phonon line in the low-temperature Cr^{3+} luminescence spectrum ($^2E \rightarrow {}^4A_2$ transition) in $Cr^{3+}:Cs_2NaGaF_6$ only observed for the center with the shortest fluorescence lifetime, has been considered as an additional argument to identify this center as Cr^{3+} at $M2$, the site with the larger axial distortion.[12] However, it should be noted that group theory does not predict an E level splitting when symmetry changes from O_h to D_{3d} or C_{3v}. Of course, the observed splitting may result from spin orbit coupling and/or Jahn-Teller effects, but then there are no arguments why it would be observed for only one of the Cr^{3+} centers. Indeed, in $Cr^{3+}:Cs_2NaAlF_6$ both centers exhibit a nearly identical splitting of the zero phonon lines,[11] while their D parameters are significantly larger, but still comparable in magnitude to those of the corresponding centers in $Cr^{3+}:Cs_2NaGaF_6$.[18] An identification solely based on fluorescence lifetime also ignores possible lattice distortions due to the Cr^{3+} incorporation.

In this work, a direct site identification of the Cr^{3+} centers in $Cr^{3+}:Cs^2NaAlF_6$ and $Cr^{3+}:Cs_2NaGaF_6$ is achieved by observing the interactions of neighboring nuclei (all nuclei in the crystals have nuclear spin) with the paramagnetic electrons of Cr^{3+} using ENDOR. The analysis of the interactions with the first ^{19}F and nearest ^{23}Na shells provide sufficient information for an unambiguous site identification. The results confirm the earlier assignations from EPR measurements.[17,18] The (super)hyperfine and quadrupole parameters determined for the aforementioned nuclei, and for the central ^{53}Cr nucleus, are correlated with the crystallographic data[14,15] for the two M^{3+} sites in the hexagonal elpasolite lattices. A tentative correlation between the EPR and optical spectroscopy data is given as well.

EXPERIMENTAL DETAILS

The Cs_2NaAlF_6 and Cs_2NaGaF_6 crystals investigated in this study were hydrothermally grown[11,12] and doped with approximately 0.1 at. % Cr^{3+}. EPR and ENDOR spectra were recorded at X band (9.56 GHz) on a Bruker ESP300E spectrometer with a ESP353 ENDOR-Triple extension, equipped with an Oxford ESR910 flow cryostat (2–300 K) and at Q band (34.0 GHz) on a Bruker Elexsys E500 spectrometer equipped with an Oxford CF935 cryostat (4.2–300 K).

Crystals of about $3\times3\times1$ mm^3 with natural faces were selected for X-band experiments. The crystals were oriented in the cavity by inspection of their EPR spectra. The X-band setup allows rotation of the crystal around one axis and tilting of this axis over a limited angular range. In this way, the crystals can be oriented to their c axis with an accuracy estimated at 0.25°. For recording the angular dependences of the X-band spectra, the samples were oriented with their c axis along the static magnetic field ($\alpha=0°$), and then rotated with 5° intervals to an arbitrary direction in the ab plane ($\alpha=90°$). The samples used for Q-band measurements ($1\times1\times3$ mm^3) were cut from oriented X-band samples. The Q-band setup does not allow any tilting of the rotation axis. As a result the crystals cannot be accurately oriented to their c axis. Angular dependences of the spectra were taken starting from the orientation closest to the c axis, and rotating the crystal with 5° intervals over 90° (arbitrary direction in the ab plane) or 180° (magnetic field approximately parallel with the $-c$ axis).

EPR spectra were recorded, modulating the static magnetic field at 12.5 kHz (X band) and 87.5 kHz (Q band) with an amplitude of 0.05–0.10 mT. The ENDOR spectra were recorded modulating the rf frequency at 12.5 kHz with a depth of 20–100 kHz. Some spectra were recorded modulating the amplitude of the rf field, resulting in nonderivative spectra.

EXPERIMENTAL RESULTS

EPR results

For the two crystals, EPR spectra were taken at X- and Q-band microwave frequencies at room temperature ($\approx$300 K) and 20 K. In Fig. 2, the X-band spectra at 20 K for the Cs_2NaGaF_6 crystal with the magnetic field parallel

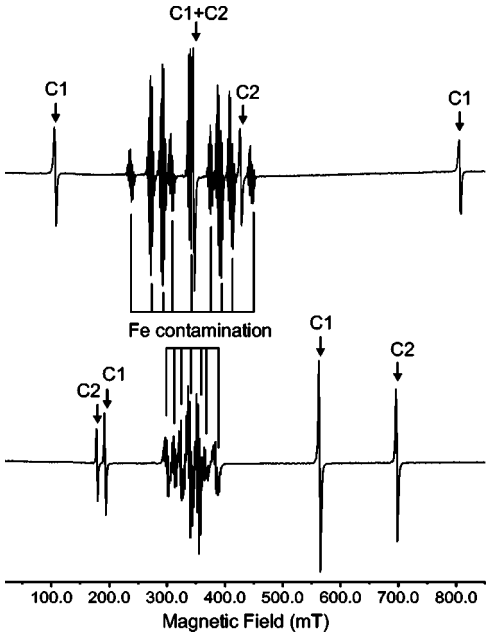

FIG. 2. Single crystal *X*-band (9.56 GHz) EPR spectrum of Cr^{3+}-doped Cs_2NaGaF_6, recorded at 20 K with the magnetic field parallel (upper trace) and perpendicular (lower trace) to the *c* axis. Transitions due to the two Cr^{3+} centers in these crystals are marked *C*1 or *C*2, the transitions due to the Fe^{3+} impurity in the crystals are indicated as well.

and perpendicular to the *c* axis are shown and the transitions assigned to the centers *C*1 and *C*2 are indicated. Apart from these, a large number of lines centered around $g \approx 2$ appear, which can be clearly distinguished from the Cr^{3+} transitions due to their smaller linewidth. These are attributed to an Fe^{3+} contamination of the crystals and will not be further analyzed here. The parameters $g_{\|}$, $g_{\perp}$, and *D* for the centers *C*1 and *C*2 were determined by least squares fitting the resonance magnetic field positions calculated by diagonalization of the axial spin Hamiltonian[22]

$$\hat{H}_S = \mu_B(g_{\|}B_z\hat{S}_z + g_{\perp}B_x\hat{S}_x) + \frac{D}{3}(3\hat{S}_z^2 - \hat{S}^2) \qquad (1)$$

($S=3/2$) to the transition fields observed in these *X*-band spectra. In Eq. (1), μ_B represents the Bohr magneton. The resulting values for the two crystals at the mentioned temperatures are collected in Table I. As an example for the quality of the fit, the angular variations of the *X*- and *Q*-band spectra for $Cr^{3+}:Cs_2NaAlF_6$ at room temperature are presented in Fig. 3, along with simulations using the best fit parameters.

Inspection of the results in Table I shows that for all centers the *g* tensors are nearly isotropic and nearly independent of temperature. The principal values are chosen to be positive, in accordance with the perturbation theory results for these ions.[22] As previously reported for $Cr^{3+}:Cs_2NaGaF_6$ powders,[18] the temperature dependence of the zero field splitting parameter is significant. For the centers in Cs_2NaAlF_6, it is less pronounced than in the other crystal, though. The choice for the signs will be substantiated below.

TABLE I. EPR spin Hamiltonian parameters for Cr^{3+} centers in Cs_2NaAlF_6 and Cs_2NaGaF_6. Experimental errors are indicated as a subscript. *D* values are given in MHz. Signs between brackets indicate that only absolute values were determined. The temperatures (in K), to which the parameters refer, are stated between brackets.

	Cs_2NaAlF_6		Cs_2NaGaF_6	
	*C*1	*C*2	*C*1	*C*2
$g_{\|}(20)$	1.9735_5	1.9730_5	1.9740_5 1.973_3[b]	1.9728_5 1.973_3[b]
$g_{\perp}(20)$	1.9738_5	1.9748_5	1.9736_5 1.973_3[b]	1.9751_5 1.973_3[b]
$g_{\|}(300)$	1.9731_5 1.97[a]	1.9743_5 1.97[a]	1.9722_5 1.973_3[b]	1.9719_5 1.973_3[b]
$g_{\perp}(300)$	1.9737_5 1.97[a]	1.9744_5 1.97[a]	1.9728_5 1.973_3[b]	1.9747_5 1.973_3[b]
$D(20)$	-7653_{10}	11726_{10}	-6267_{12} -6270_{60}[b]	10683_{12} 10680_{60}[b]
$D(300)$	-7766_{10} (−)7650[a]	11786_{10} (+)11760[a]	-6472_{12} -6495_{60}[b]	10871_{12} 10890_{60}[b]

[a]Fargin *et al.*, Ref. 17.
[b]Vrielinck *et al.*, Ref. 18.

It should further be noted that our EPR results agree within experimental accuracy with those earlier reported.[17,18]

For both centers in both crystals, the zero field splitting of the ground-state multiplet (2D) is slightly larger than the *X*-band microwave quantum. As a result, for arbitrary magnetic field orientations, only a limited number of EPR transitions can be observed, whose transition probabilities are strongly angular dependent. At *Q*-band frequencies, 2D is appreciably smaller than the microwave quantum. For all magnetic field orientations, three "allowed" ($\Delta M_S=1$) transitions with high intensity can be detected, although their transition field may be situated above the limits of the experimental setup [Fig. 3(b)]. In addition, several "forbidden" transitions ($\Delta M_S=2,3$) are observed in the low magnetic field range with lower intensity (transition probability). Moreover, the signal to noise ratio of the Cr^{3+} spectra is much higher at *Q* than at *X* band. It further turns out that the intensity of the ENDOR spectra is also much higher at *Q* band. As a result, except for the first shell ^{19}F interaction for *C*2 where the ENDOR transitions could be followed throughout the complete angular range at *X* band, angular variations of the ENDOR spectra could only be recorded at *Q* band. In view of the higher accuracy in orienting the crystals, where possible the spin Hamiltonian parameters have been extracted from *X*-band ENDOR spectra.

ENDOR results

All *X*- and *Q*-band ENDOR spectra were recorded at 20 K. In Fig. 4 the *Q*-band ENDOR spectra of $Cr^{3+}:Cs_2NaGaF_6$, recorded with the magnetic field perpendicular to the *c* axis at the central "allowed" EPR transition of the centers *C*1 and *C*2 are shown. As indicated, for each center transitions due to the central ^{53}Cr ($I=3/2$, 9.5% natu-

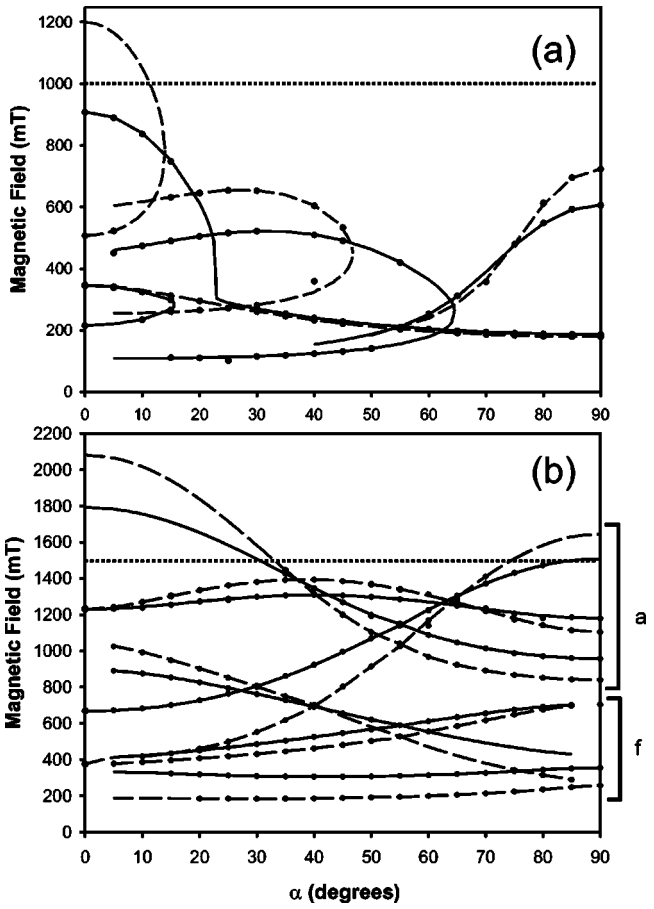

FIG. 3. Angular dependence of (a) the *X*-band (9.56 GHz) and (b) the *Q*-band (34.00 GHz) EPR spectrum of $Cs_2NaAlF_6:Cr^{3+}$, recorded at room temperature. Filled circles represent experimental data points. The simulated angular dependences, using the data in Table I, are represented by the full (*C*1) and dashed (*C*2) lines. 0° refers to the *c* axis and 90° to an arbitrary direction in the *ab* plane. The experimental magnetic field limit of the setup is indicated with a dotted line. In the *Q*-band angular dependence ($h\nu_{MW} > 2D$) the "allowed" (corresponding to $\Delta M_S = 1$ at $\vec{B} \| c$) and "forbidden" transitions are marked *a* and *f*, respectively.

ral abundance) nucleus and several neighboring shells of ^{19}F ($I=1/2$), ^{23}Na ($I=3/2$), and ^{133}Cs ($I=7/2$) nuclei, are observed. The assignations to various types of nuclei were made using the magnetic field shift method.[23] The spin Hamiltonian parameters for one particular nucleus were determined by least squares fitting the transition frequencies calculated by diagonalization of the spin Hamiltonian

$$\hat{H}_S = \mu_B(g_\parallel B_z \hat{S}_z + g_\perp B_x \hat{S}_x) + \frac{D}{3}(3\hat{S}_z^2 - \hat{S}^2) + \hat{\vec{S}} \cdot \overleftrightarrow{A} \cdot \hat{\vec{I}}$$
$$- g_N \mu_N \vec{B} \cdot \hat{\vec{I}} + \hat{\vec{I}} \cdot \overleftrightarrow{Q} \cdot \hat{\vec{I}} \qquad (2)$$

to the experimental frequencies, using the EPR data in Table I and the known g_N value for each nucleus.[24] In addition to the terms in Eq. (1), spin Hamiltonian (2) includes the (super)hyperfine [(s)hf] interaction, the nuclear Zeeman interaction (μ_N: nuclear magneton) and the quadrupole interaction, which only has a nonzero contribution if $I > 1/2$. The best fit interaction parameters are shown in Table II.

As will be substantiated below, the analysis of the interaction with the first ^{19}F shell and with the nearest ^{23}Na shell allows to identify the position of the Cr^{3+} ion for the two centers in an unambiguous way. The ^{53}Cr hf interaction, on the other hand, enabled us to determine the sign of the zero field splitting parameter and the shf interaction parameters. The interactions with the ^{133}Cs nuclei do not supply additional information necessary for the site assignations. As these spectra were only poorly resolved, they have not been further analyzed.

^{53}Cr hyperfine interaction

^{53}Cr has nuclear spin 3/2. At each EPR transition, two triplets of lines, corresponding to the ENDOR transitions within the two M_S multiplets should thus be observed, as shown in Fig. 4. Due to the low natural abundance of this isotope (9.5%), which is also partly responsible for the low intensity of the ENDOR transitions, and to the relatively large width of individual EPR lines, this interaction is not resolved in the EPR spectra.

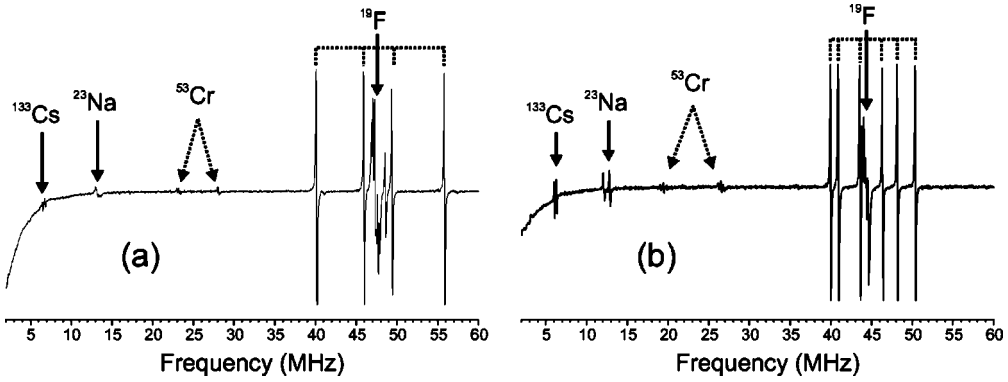

FIG. 4. *Q*-band (34.00 GHz) ENDOR spectra, recorded at 20 K with $\vec{B} \perp c$ at (a) $B = 1182$ mT (*C*1) and (b) 1107 mT (*C*2). Transitions assigned to the nearest ^{133}Cs, ^{23}Na shells and the second (and further) ^{19}F shells are close to the Larmor frequencies of the respective nuclei, indicated with straight arrows. Transitions due to the interaction with the central ^{53}Cr nucleus and to the first ^{19}F shell are also indicated (dotted lines).

TABLE II. shf and quadrupole principal values (in MHz) and declination angles (in degrees) for the interactions of the unpaired electrons with the central ^{53}Cr and the nearest ^{19}F and ^{23}Na neighboring shells of nuclei for the $C1$ and $C2$ centers in Cs_2NaAlF_6 and Cs_2NaGaF_6. The principal directions corresponding to A_x or Q_x are perpendicular to the center's symmetry plane containing the interacting nucleus and the central Cr^{3+} ion and $\theta_{A/Q}$ is the angle between the principal A_z/Q_z direction and the c axis. Signs between brackets could not be experimentally determined. All parameters are determined at 20 K. Errors are indicated as a subscript.

		Cs_2NaAlF_6		Cs_2NaGaF_6	
		$C1$	$C2$	$C1$	$C2$
^{53}Cr	$A_\perp$	53.53_4	51.85_4	53.56_4	51.99_2
	$A_\parallel$	52.81_4	53.15_4	52.99_4	53.13_4
	$Q_\perp$	0.075_{15}	-0.135_{15}	0.060_{15}	-0.115_5
	$Q_\parallel$	-0.15_3	0.27_3	-0.12_3	0.23_1
^{19}F	A_x	7.35_{40}	12.06_6	6.56_{40}	12.05_4
	A_y	8.00_{20}	10.82_{11}	7.94_{20}	11.03_8
	A_z	-28.53_{40}	-27.72_7	-27.96_{40}	-27.75_4
	θ_A	56.1_5	51.1_3	55.8_5	50.9_2
^{23}Na	A_x	-0.53	-0.80_1	-0.50	-0.87_1
	A_y	-0.53	-0.80_1	-0.50	-0.87_1
	A_z	0.20	1.44_1	0.00	1.42_1
	θ_A	60	0	52	0
	Q_x	(−)0.03	$(-)0.019_5$		$(-)0.006_2$
	Q_y	(−)0.03	$(-)0.019_5$		$(-)0.006_2$
	Q_z	(+)0.06	$(+)0.038_7$		$(+)0.012_3$
	θ_Q	20	0		0

In Fig. 5 the angular dependence of the ^{53}Cr ENDOR transitions, recorded at Q band by saturating the EPR transition corresponding to $M_S: 1/2 \leftrightarrow -1/2$ for $\vec{B} \| c$, is shown for the two centers in the two crystals. The best fit hf and quadrupole parameters for this interaction, determined from the X-band spectra with $\vec{B} \| c$ and $\vec{B} \perp c$, are listed in Table II. The agreement of the calculated angular dependence with the experimental results at Q band demonstrates the consistency of the analysis.

Considering the spin Hamiltonian parameters in Table II, for both centers in both crystals, the hf tensor is nearly isotropic, although the ENDOR transition frequencies strongly depend on the magnetic field orientation. This is primarily due to the large zero field splitting, as a result of which the various M_S states are strongly mixed for $\vec{B} \| c$ and the saturated EPR transition shows a pronounced angular dependence [see Fig. 3(b)]. In various environments, the hf tensor for Cr^{3+} centers has been found to be dominated by the core polarization contribution, leading to principal values of approximately +50 MHz (Refs. 25–27) ($g_N = -0.3147$). In view of these results, it may safely be assumed that the hf values in Table I are positive. The signs of the quadrupole values have been determined relative to that of the second order hf contribution ($\sim A_{\rm iso}^2/h\nu_{\rm MW}$) to the triplet splitting of the ^{53}Cr transitions corresponding to each M_S multiplet[27] and have been checked by ENDOR-induced EPR measurements.

The knowledge of the sign for the hf interaction allows us to determine the signs of the zero field splitting parameters, by recording the spectra at different EPR transitions. Previously,[18] we have already used this procedure to determine the signs of D for the two centers in Cs_2NaGaF_6 from Q-band powder ENDOR spectra. Figure 6 shows the high frequency part of the Q-band spectra with the magnetic field approximately parallel to the c axis for $C1$ and $C2$ in Cs_2NaAlF_6 recorded at the $|M_S| = 3/2 \leftrightarrow |M_S'| = 1/2$ transition at low field. The first order perturbation expression for the transition field at which these spectra are recorded, is given by[23]

$$B = \frac{h\nu_{\rm MW} - D(M_S + M_S')/2}{g_\parallel \mu_B}, \tag{3}$$

whereas the first order expression for the ENDOR frequency of the allowed $M_I \leftrightarrow M_I'$ transition ($\Delta M_I = 1$) within the M_S multiplet is given by

$$\begin{aligned} h\nu &= |A_\parallel M_S - g_N \mu_N B + 3Q_\parallel (M_I + M_I')| \\ &= \frac{3}{2}A_\parallel \mp g_N \mu_N B \pm 3Q_\parallel (M_I + M_I') \end{aligned} \tag{4}$$

as the high frequency resonances correspond to transitions within the $M_S = \pm 3/2$ multiplet. Because the hf values are positive, the g_N factor is negative and $3Q < g_N \mu_N B$, for a positive D the transition frequencies all lie above $\frac{3}{2}A_\parallel$, as is observed for $C2$ [Fig. 6(c)], and they all lie below this value for a negative D, as for $C1$ [Fig. 6(b)]. The sign of all shf interaction parameters can be determined in a similar way, now knowing the sign of D for each center.

^{19}F interaction

^{19}F has nuclear spin $1/2$, so two ENDOR transitions are expected for each set of equivalent nuclei (one transition within each of the M_S multiplets between which the EPR transition is saturated). The angular dependences of the spectra were recorded by saturating the EPR transition corresponding to $M_S: 1/2 \leftrightarrow -1/2$ for $\vec{B} \| c$. In the Q-band ENDOR spectra, a large number of transitions are observed, which remain close to the ^{19}F larmor frequency (indicated in Fig. 4) for all magnetic field orientations. These are due to interactions of the unpaired electrons with remote ^{19}F nuclei (second and further shells). As these transitions were only poorly resolved, no attempt was made to analyze them.

Apart from these, in the Q-band ENDOR spectra for an arbitrary magnetic field orientation, six transitions occur at frequencies more deviant from the Larmor frequency, and show a pronounced angular dependence. These are assigned to the interaction with the nearest ^{19}F nuclei, which apparently belong to three magnetically inequivalent sets. Their complete angular dependence (180° interval) for the $C1$ centers in both crystals are shown in Figs. 7(a) and 7(c), along with simulations using the spin Hamiltonian values in Table II, assuming that the three inequivalent sets of nuclei belong to the same shell. This implies that these sets (and their shf tensors) are transformed into one another by rotations over

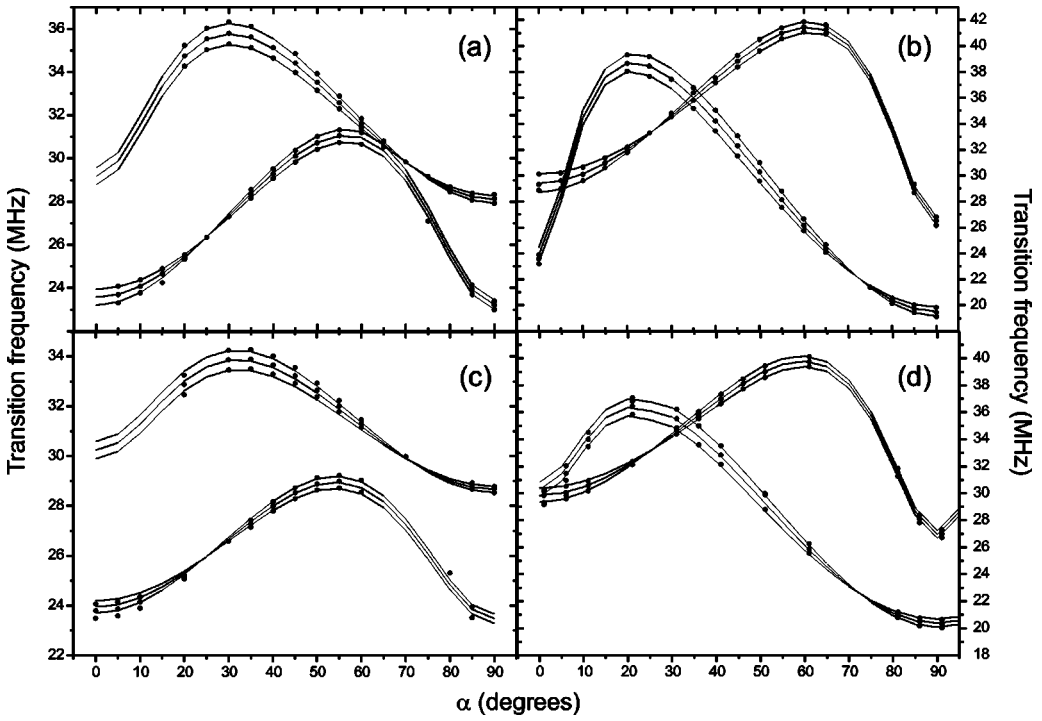

FIG. 5. Angular variation of the *Q*-band ^{53}Cr ENDOR spectra, recorded at 20 K, for (a) *C*1 and (b) *C*2 in Cs_2NaAlF_6 and for (c) *C*1 and (d) *C*2 in Cs_2NaGaF_6. Filled circles represent experimental data points and the full lines are calculated angular dependences using the *A* and *Q* values in Table III. At 0°, the magnetic field is approximately parallel to the *c* axis and 90° corresponds to an arbitrary direction in the *ab* plane.

±120° around the *c* axis. For $\vec{B}\|c$ all nuclei in this shell become magnetically equivalent and the transitions for the three sets should coincide. As the *Q*-band samples could not be accurately oriented to their *c* axis, this coincidence does not actually occur in Figs. 7(a) and 7(c). From the angular dependence of the EPR transitions, the mistilt of the *c* axis could be determined and was taken into account in the simulation and fitting procedures.

For the *C*2 centers in both crystals, the angular dependence of the spectra corresponding to this interaction could also be recorded at the *X* band. The saturated EPR transition also corresponds to $M_S: 1/2 \leftrightarrow -1/2$ for $\vec{B}\|c$, but for arbitrary magnetic field orientations only three ENDOR transitions, corresponding to the lower M_S multiplet ($-1/2$ for $\vec{B}\|c$), are observed. Recording the angular dependence in a 90° interval at *X* and *Q* band proved sufficient to determine the corresponding shf tensors with high accuracy. In Figs. 7(b) and 7(d) the experimental and simulated (shf parameters in Table II) *X*-band angular variations for the two crystals are shown. The angular pattern can again be perfectly reproduced assuming that the three sets belong to the same shell of neighboring nuclei, and at 0° ($\vec{B}\|c$) the three ENDOR transitions practically coincide, showing that the crystals could be oriented to their *c* axis very accurately.

Figure 8 shows the local environment for the five inequivalent cation positions in hexagonal elpasolite crystals. For the two Cs^+ positions, the nearest F^- ions belong to three shells, one containing six and two containing three magnetically inequivalent nuclei, for the Na^+ postion, the nearest fluorine ions belong to two inequivalent shells of three ions, and for the two M^{3+} positions all six nearby anions belong to the same shell and are pairwise magnetically equivalent, due to the inversion symmetry of these sites. The fact that only one nearby anion shell is observed, already seems to prove the Cr^{3+} substitution on the tervalent cation sites. Nonetheless, the ^{19}F ENDOR results are in principle consistent with substitution on the monovalent cation sites as well, because for each of these sites, the nearest F^- shell consists of three (magnetically inequivalent) ions. Providing unambiguous proof for the substitution at the M^{3+} sites thus implies determining the total number of interacting nuclei in the first shell, which cannot be done from the ENDOR data alone. However, by simulating the shf structure in the EPR spectra, observed for some magnetic field orientations (see Fig. 9), this missing information can be inferred.

In Fig. 7(a), one observes that for the *C*1 center in the 30°–60° angular range the interaction with one of the ^{19}F sets is much larger than that with the other two, and one may expect it to be resolved in the *Q*-band EPR spectra. This shf structure, shown in Fig. 9(a), is clearly seen to exhibit a 1:2:1 intensity ratio, indicative of an interaction with two equivalent nuclei. This means the first shell consists of six rather than three ions, so the *C*1 center has local D_{3d} symmetry and Cr^{3+} is substituted on an M^{3+} position. The shf structure simulation including all six nuclei in the first shell, shown in the lower trace of Fig. 9(a) reproduces the experimental EPR spectrum fairly well. For the *C*2 center, the *X*-band EPR spectrum with $\vec{B} \perp c$ exhibits a partially resolved, more complex shf structure, which can again be fairly well reproduced assuming an interaction with six pairwise equivalent nuclei, as can be seen in Fig. 9(b). So also for *C*2, the Cr^{3+} ion is

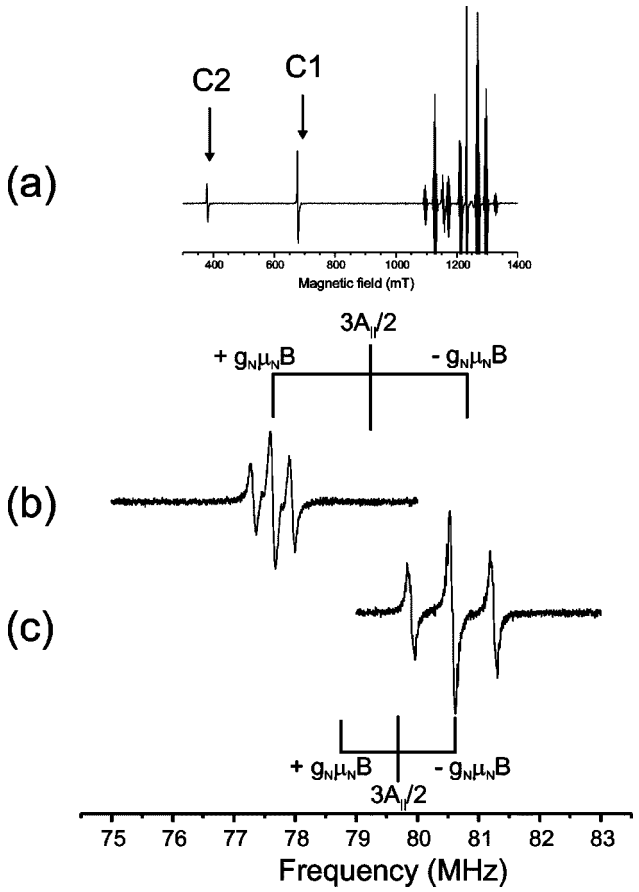

FIG. 6. (a) Q-band EPR spectrum of Cr^{3+}:Cs_2NaAlF_6 with the magnetic field approximately parallel to the c axis and high frequency part of the ^{53}Cr ENDOR spectrum recorded at the positions marked (b) $C1$ and (c) $C2$ in (a). As explained in the text, the occurrence of transitions centered at $3A_{\|}/2+g_N\mu_N B$ for $C1$ demonstrates that D is negative in this case, whereas the transitions for $C2$ are centered at $3A_{\|}/2-g_N\mu_N B$ as expected for a center with positive D.

incorporated at a site with D_{3d} symmetry, thus an M^{3+} site. The shf EPR results are only shown for the Cs_2NaAlF_6 crystal, but are very similar for the other crystal.

^{23}Na interaction

^{23}Na has $I=3/2$, and for each set of magnetically equivalent nuclei a six line pattern (similar to that observed for ^{53}Cr) is expected. Figure 10 shows the angular variation of the ^{23}Na ENDOR transitions, recorded at Q band by saturating the EPR transition corresponding to $M_S: 1/2 \leftrightarrow -1/2$ for $\vec{B}\|c$, for the two centers in the two crystals.

For the $C2$ center [Figs. 10(b) and 10(d)], the complete angular pattern is recorded in the $0°-90°$ interval and can be reproduced assuming an interaction with a single ^{23}Na nucleus located on the c axis, using the shf and quadrupole data in Table II, which were extracted from the X-band ENDOR spectra recorded with $\vec{B}\|c$ and $\vec{B}\perp c$. In these X-band spectra, the quadrupole splitting of the ENDOR transitions for $C2$ in Cs_2NaGaF_6, not resolved at Q band [see Fig. 10(d)], was also observed. Knowing this center has D_{3d} symmetry from the analysis of the first shell ^{19}F interaction, it is clear that the nearest ^{23}Na shell consists of two magnetically equivalent ions on the c axis. This unambiguously identifies the $C2$ center as Cr^{3+} incorporated at position $M2$.

TABLE III. Interionic distances (R) and declination angles (θ) calculated for the first F^- and Na^+ shells around the M^{3+} ions in Cs_2NaAlF_6 and Cs_2NaGaF_6, based on crystallographic data in Refs. 14 and 15, respectively. Distances are given in nm and angles in degrees. The errors are estimated at one unit in the last digit.

	Cs_2NaAlF_6		Cs_2NaGaF_6	
	$M1$	$M2$	$M1$	$M2$
$R_{M\text{-}F}$	0.182	0.181	0.190	0.190
$\theta(c, M\text{-}F)$	55.0	53.3	55.2	53.2
$R_{M\text{-Na}}$	0.412	0.293	0.417	0.296
$\theta(c, M\text{-Na})$	60.3	0	60.0	0

For $C1$, the ^{23}Na ENDOR spectra are weak and show rather poor resolution. In Cs_2NaGaF_6 [Fig. 10(c)], for most magnetic field orientations, only two broad and asymmetrically shaped transitions can be observed in the frequency modulated spectra. By recording with amplitude modulation, it was checked for some magnetic field orientations that the nonderivative spectra are the result of a superposition of nonresolved transitions, of which only the extreme positions can be observed in the frequency modulated first derivative spectra. In Cs_2NaAlF_6 an additional splitting of the ENDOR transitions occurs, which we attribute to the quadrupole interaction. At X band, for no magnetic field orientation the ^{23}Na interaction could be detected for this center.

Having only a limited set of poorly resolved ENDOR lines, it was impossible to obtain a unique set of spin Hamiltonian parameters for this interaction. Nonetheless, it could unambiguously be determined from the angular variation that the interacting nuclei are not located on the c axis, and hence, the shell should consist of six ions. Therefore, $C1$ can unambiguously be identified as Cr^{3+} incorporated at position $M1$. Assuming an interaction with six pairwise equivalent ^{23}Na nuclei at the same azimuthal angles as the first shell ^{19}F nuclei, a reasonably good agreement between experimental and calculated angular variations for this interaction is obtained using the spin Hamiltonian parameters in Table II. The considerably smaller shf tensor anisotropy as compared to the ^{23}Na interaction for $C2$, gives additional support to the assignation, because in the former center the interacting nuclei are at a much larger distance than in the latter.

DISCUSSION

As mentioned in the Introduction, the assignations of the optical absorption and emission spectra to the two centers critically depend on the assumption that the Cr^{3+} ions do not too much disturb the symmetry at the site where they are incorporated. Having identified the Cr^{3+} lattice position for each center, we may try to evaluate this assumption by comparing the spin Hamiltonian parameters obtained in this study with those expected for the unrelaxed lattice. For both

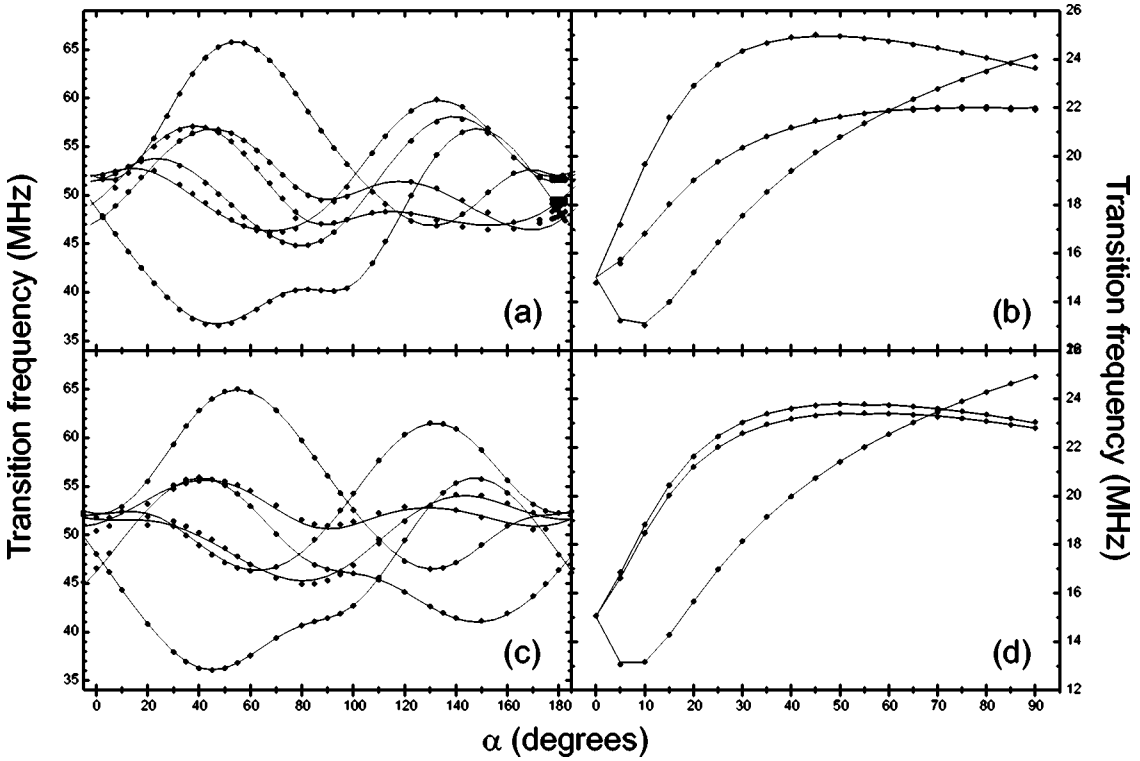

FIG. 7. Angular dependence of the first shell ^{19}F ENDOR spectra for (a) $C1$ and (b) $C2$ in Cs_2NaAlF_6 and for (c) $C1$ and (d) $C2$ in Cs_2NaGaF_6. All ENDOR spectra were recorded at 20 K, at Q band for the $C1$ center and at X band for $C2$. Filled circles represent experimental data points and the full lines are calculated angular variations using the data in Table II. At 0° and 180° the magnetic field is approximately parallel to the c axis and 90° corresponds to an arbitrary orientation in the ab plane.

M^{3+} positions in both crystals, the positions of the nearest ^{19}F and ^{23}Na ions, calculated from the single crystal x-ray or neutron diffraction data,[14,15] are listed in Table III. Direct ways of connecting the optical and structural data for the two centers would require optically detected magnetic resonance (ODMR) experiments or quantum chemical calculations, neither of which have been performed in this study.

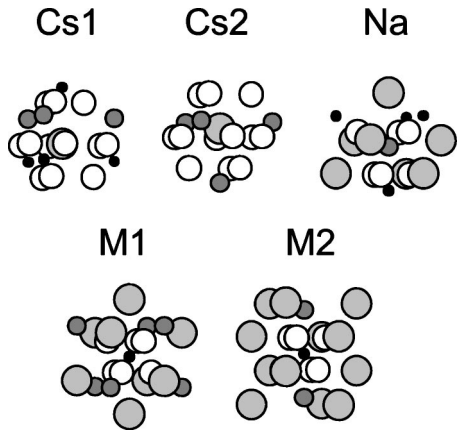

FIG. 8. Lattice surroundings of the five inequivalent cation positions in the Cs_2NaMF_6 crystals. The labeling of the sites is defined in Fig. 1. The two Cs^+ positions have three nearby ^{19}F shells consisting of 3 (closest), 6 and 3 (most distant) magnetically inequivalent nuclei. The Na^+ position has two nearby ^{19}F shells, each consisting of three magnetically inequivalent nuclei. Both M^{3+} positions have six pairwise magnetically equivalent ^{19}F nuclei in the first shell.

McGarvey[25] and Manoogian and Lecle[26] have related the signs of the zero field splitting, the anisotropic hf $[A_a=(A_\parallel-A_\perp)/3]$ and quadrupole $(q=-Q_\perp=Q_\parallel/2)$ parameters for the ^{53}Cr nucleus to the trigonal distortion of the first anion (O^{2-}, in their case) shell. In a strong octahedral crystal field, whereon a small trigonal distortion is superimposed, it has been found that a trigonal compression leads to negative D and A_a and to a positive q, whereas opposite signs for all these parameters should be found for trigonally elongated sites. From the data in Table III, we may conclude that at the undistorted position $M1$ the first shell octahedron is slightly compressed ($\theta>54.7°$, as for the regular octahedron) in both crystals, whereas at site $M2$ it is slightly elongated. In agreement with findings of McGarvey, D and A_a are negative for the $C1$ centers and positive for the $C2$ centers. For q, however, a discrepancy with the results of Manoogian and Leclerc is found. Probably, in the present case, the quadrupole values exhibit non-negligible influences from more distant shells of nuclei.

The distortion of the first anion shell may also be evaluated through the shf tensors of the nearest ^{19}F nuclei. In view of the large negative anisotropic part of these tensors (in spite of the positive g_N for ^{19}F), it is reasonable to assume that they are dominated by overlap and covalency contributions. An analysis in terms of a simple point dipole interaction between the unpaired electrons and the ^{19}F nucleus is therefore useless. We may, however, still expect that the prin-

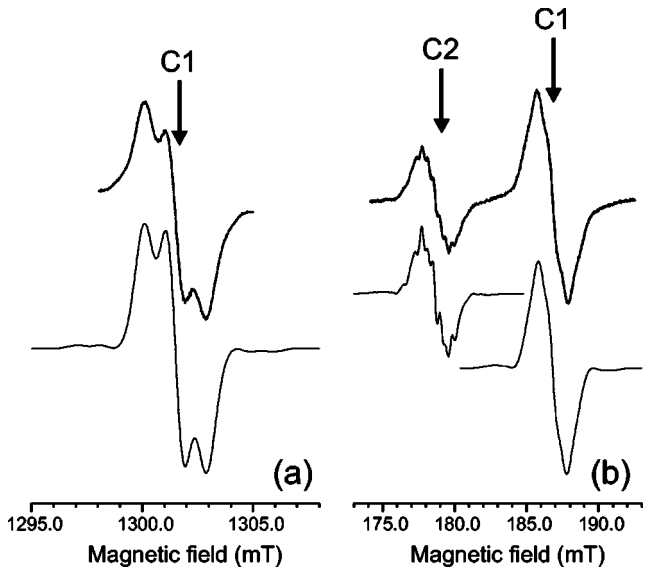

FIG. 9. Experimental (upper traces, recorded at 20 K) and simulated (lower traces) EPR spectra of Cr^{3+}:Cs_2NaAlF_6 exhibiting a partially resolved shf structure due to the interaction with the first ^{19}F shell. (a) *Q*-band (34.00 GHz) spectrum at $\alpha=52°$ [see Fig. 7(a)] for *C*1, (b) *X*-band (9.56 GHz) spectrum at $\alpha=90°$ [see Fig. 7(b)] for *C*2 and *C*1. The *C*1 spectra show a partially resolved 1:2:1 shf pattern, indicative of a dominant interaction with two magnetically equivalent ^{19}F nuclei. The *C*2 shf pattern is more complex. All simulations include the interactions with three magnetically inequivalent pairs of equivalent ^{19}F nuclei and with the central ^{53}Cr nucleus ($I=3/2$, 9.5% natural abundance) using the shf data in Table II. The simulations were performed by calculating the splittings due to the ^{53}Cr ion and to each pair of equivalent ^{19}F nuclei separately, superimposing the patterns afterwards.

cipal direction corresponding to the largest principal value (absolute value) is approximately parallel to the Cr^{3+}-F^- bond axis. The declination angles for the shf tensors again indicate that the Cr^{3+} ion in the *C*1 center has a compressed octahedral environment, whereas that for *C*2 is elongated. The deviations from $\theta=54.7°$ are larger for the shf tensors than for the ionic positions of the unrelaxed first shell. This might be a result of a relaxation of this shell but may even well be accounted for by covalency effects. Furthermore, it should be noted that the crystallographic data refer to room temperature, whereas the ENDOR spectra were recorded at 20 K.

All parameters related to the trigonal distortion of the first coordination shell ($|D|$, $|A_a(^{53}Cr)|$, $|q(^{53}Cr)|$, $|\theta_A(^{19}F)-54.7°|$) are larger for *C*2 than for *C*1, thus strongly indicating that the deviation from cubic symmetry is larger for *C*2 than for *C*1. Also for the undistorted lattice sites, the deviation from octahedral coordination ($|\theta(F^-)-54,7°|$) is larger for *M*2 than for *M*1.

For the nearest ^{23}Na nuclei, which are located farther away from the unpaired electrons than the first ^{19}F shell, a point dipole analysis might be useful. In the *C*2 center, assuming the anisotropic shf interaction is completely accounted for by the point dipole contribution, the Cr^{3+}-Na^+ distance is calculated to be 0.302 nm for Cs_2NaAlF_6 and 0.300 nm for Cs_2NaGaF_6. These values correspond well with the crystallographic data (see Table III), taking into account the difference in temperature at which the two sets of data were determined and the fact that there is probably also a small (negative) contribution due to overlap or covalency effects, judging from the small negative isotropic shf constant. For the *C*1 center the Cr^{3+}-Na^+ distances calculated for the two crystals within the point dipole approximation (0.439 nm and 0.498 nm, for Cs_2NaAlF_6 and Cs_2NaGaF_6, respectively) do not present an equally satisfactory agreement with the crystallographic data (see Table III). For the center in Cs_2NaGaF_6, the declination angle θ_A does not correspond to the angle between the Cr^{3+}-Na^+ interconnection line and the *c* axis. Apparently, the point dipole interaction does not account for the complete anisotropic part of the shf tensor in this case. It should be born in mind, though, that we did not find a unique fitting of the data, and therefore choose not to put error margins for these values. In addition, the larger negative isotropic shf value (as compared with that for the ^{23}Na interaction for *C*2) may also result from a larger influence of overlap and covalency effects. This may find its origin in direct overlap with the *s* and *p* orbitals of the nearest F^- anions. For Rh and Ir chlorocyanide complexes in alkali halides similar effects have given rise to a so-called super-superhyperfine structure in the EPR spectra.[28]

So far, the comparison between crystallographic and ENDOR data indicate that the symmetry of the M^{3+} sites is not significantly disturbed by the Cr^{3+} substitution. In this sense, ENDOR appears to support the assignations of the optical transitions based on luminescence lifetime measurements. They should, however, preferably be directly checked experimentally or through calculations.

Aramburu *et al.*[29] and Barriuso *et al.*[30] have theoretically explored the influence of the transition-metal–fluoride distance on spectroscopic properties, e.g., the crystal-field splitting 10 Dq and the isotropic shf constant, and found pronounced dependences. For the dependence of 10 Dq on the M^{3+}-F^- distance it has been pointed out in a previous study[18] that, when comparing the data for the same center, larger values for this optical parameter are found in Cs_2NaAlF_6 than in Cs_2NaGaF_6. Comparing the ^{19}F shf data for the corresponding centers in the two crystals, hardly any difference is seen, in spite of the appreciable difference between the Al^{3+}-F^- and the Ga^{3+}-F^- distances. This might either mean that the shf tensors are not very sensitive to this distance, as already suggested for their isotropic part by Barriuso *et al.*,[30] or that the first F^- shell may undergo an appreciable distortion without significantly changing the degree of trigonal compression or elongation of the octahedron. We are tempted to believe the second possibility, supported by the fact that the quadrupole interaction parameters for both the ^{53}Cr and the nearest ^{23}Na nuclei are larger in the Cs_2NaAlF_6 crystal than in the other. These larger quadrupole values suggest larger lattice relaxations around the Cr^{3+} ion (leading to larger electric field gradients), which are indeed expected, as the difference in ionic radius between the Al^{3+} ion and Cr^{3+} is much larger than between Ga^{3+} and Cr^{3+}.

Apparently, the ENDOR data bear very detailed quantitative information on the geometry of the CrF_6^{3-} complexes under study, but this information is not directly accessible. Quantum chemical calculations of geometries, optical and

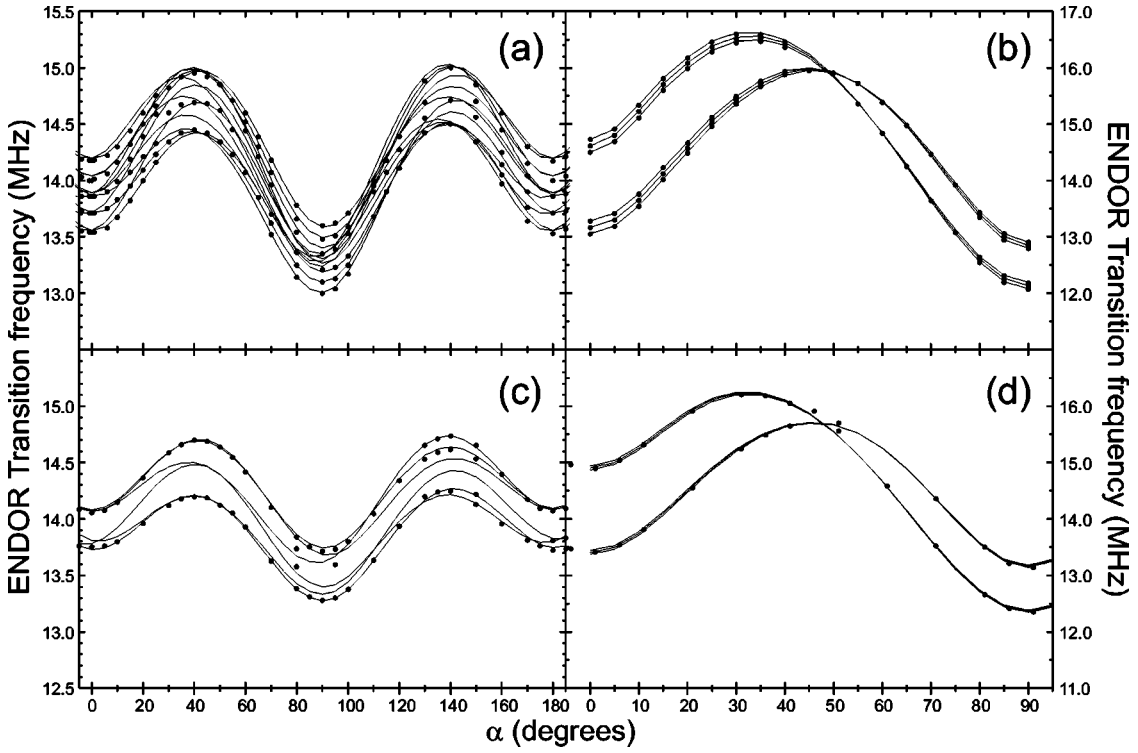

FIG. 10. Angular dependence of the *Q*-band ^{23}Na ENDOR spectrum, recorded at 20 K, for (a) *C*1 and (b) *C*2 in Cs_2NaAlF_6 and for (c) *C*1 and (d) *C*2 in Cs_2NaGaF_6. Filled circles represent experimental data points. The full lines (simulations) were calculated using the shf and quadrupole data in Table II. At 0° and 180° the magnetic field is approximately parallel to the *c* axis and 90° corresponds to an arbitrary orientation in the *ab* plane. In the spectra for Cs_2NaGaF_6 the quadrupole splitting remains unresolved at the *Q* band.

paramagnetic parameters for these centers should provide a deeper insight into various aspects pointed out above.

CONCLUSIONS

Analysis of the interaction of the unpaired electrons of two Cr^{3+} centers in Cs_2NaAlF_6 and Cs_2NaGaF_6 crystals with the first ^{19}F coordination shell and with the nearest ^{23}Na shell, as observed using ENDOR, allowed an unambiguous identification of the lattice sites at which Cr^{3+} is incorporated: in the center *C*1, with a negative zero field splitting, Cr^{3+} is located at the position *M*1, i.e., the M^{3+} position for which the MF_6 octahedron is connected to six NaF_6 octahedra through corners, and in the center *C*2, with a larger positive zero field splitting, Cr^{3+} is at position *M*2, the MF_6 octahedron being connected to two NaF_6 octahedra through faces. The signs of the zero field splitting and shf parameters have all been determined relative to that of the positive ^{53}Cr hyperfine values. Inspection of the spin Hamiltonian parameters for the ^{53}Cr nucleus and the nearest ^{19}F and ^{23}Na neighboring nuclei suggest that the Cr^{3+} incorporation induces lattice distortions, which, however, do not significantly change the degree of trigonal elongation or compression of the MF_6 octahedra in the undistorted lattice. The present ENDOR study thus supports earlier assignations of optical transitions to the two Cr^{3+} centers, based on fluorescence lifetime measurements, which should nonetheless preferably be further checked, experimentally or through calculations.

ACKNOWLEDGMENT

The authors, in particular H.V., acknowledge the Fund for Scientific Research – Flanders (Belgium) for financial support.

*Author to whom correspondence should be addressed.

[1] U. Keller, Nature (London) **424**, 831 (2003).
[2] J. M. Hopkins, G. J. Valentine, B. Agate, A. J. Kemp, U. Keller, and W. Sibbett, IEEE J. Quantum Electron. **38**, 360 (2002).
[3] B. Agate, E. U. Rafailov, W. Sibbett, S. M. Saltiel, P. Battle, T. Fry, and E. Noonan, Opt. Lett. **28**, 1963 (2003).
[4] M. Grinberg and K. Holliday, J. Lumin. **92**, 277 (2001).
[5] I. Nikolov, X. Mateos, F. Guell, J. Massons, V. Nikolov, P. Peshev, and F. Diaz, Opt. Mater. (Amsterdam, Neth.) **25**, 53 (2004).
[6] A. Caramanian, J. P. Souron, P. Gredin, A. de Kozak, J. Derouet and B. Viana, J. Lumin. **104**, 161 (2004).
[7] A. N. Medina, A. C. Bento, M. L. Baesso, F. G. Gandra, T. Catunda, and A. Cassanho, J. Phys.: Condens. Matter **13**, 8435

(2001).
[8] O. S. Wenger, R. Valiente and H. U. Gudel, J. Chem. Phys. **115**, 3819 (2002).
[9] M. Grinberg, Opt. Mater. (Amsterdam, Neth.) **19**, 37 (2002).
[10] R. H. Bartram, G. R. Wein, and D. S. Hamilton, J. Phys.: Condens. Matter **13**, 2377 (2001).
[11] L. P. Sosman, A. Dias Tavares, Jr., R. J. M. da Fonseca, T. Abritta, and N. M. Khaidukov, Solid State Commun. **114**, 661 (2000).
[12] R. J. M. da Fonseca, A. Dias Tavares, Jr., P. S. Silva, T. Abritta, and N. M. Khaidukov, Solid State Commun. **110**, 519 (1999).
[13] R. J. M. da Fonseca, L. P. Sosman, A. Dias Tavares, Jr., and H. N. Bordallo, J. Fluoresc. **10**, 375 (2000).
[14] H. N. Bordallo, R. W. Henning, L. P. Sosman, R. J. M. da Fonseca, A. Dias Tavares, Jr., K. M. Hanif, and G. F. Strouse, J. Chem. Phys. **115**, 4300 (2001).
[15] H. N. Bordallo, X. Wang, K. M. Hanif, G. F. Strouse, R. J. M. da Fonseca, L. P. Sosman, and A. Dias Tavares, Jr., J. Phys.: Condens. Matter **14**, 12383 (2002).
[16] G. A. Torchia, D. Schinca, N. M. Khaidukov, and J. O. Tocho, Opt. Mater. (Amsterdam, Neth.) **20**, 301 (2002).
[17] E. Fargin, B. Lestienne, and J. M. Dance, Solid State Commun. **75**, 769 (1990).
[18] H. Vrielinck, N. M. Khaidukov, F. Callens, and P. Matthys, Radiat. Eff. Defects Solids **157**, 1155 (2002).
[19] D. Babel, R. Haegele, G. Pausewang, and F. Wall, Mater. Res. Bull. **8**, 1371 (1973).
[20] H. Vrielinck, K. Sabbe, F. Callens, and P. Matthys, Phys. Chem. Chem. Phys. **3**, 1709 (2001).
[21] H. Vrielinck, F. Callens, and P. Matthys, Phys. Rev. B **64**, 214105 (2001).
[22] A. Abragam and B. Bleaney, *Electron Paramagnetic Resonance of Transition Ions* (Clarendon Press, Oxford, 1970).
[23] J.-M. Spaeth, J. R. Niklas, and Bartram, *Structural Analysis of Point Defects in Solids*, Vol. 43 of Springer Series in Solid-State Sciences (Springer, Berlin, 1992).
[24] Bruker EPR and NMR frequency tables.
[25] B. R. McGarvey, J. Chem. Phys. **40**, 809 (1963).
[26] A. Manoogian and A. Leclerc, Phys. Rev. B **10**, 1052 (1974).
[27] G. Malovichko, V. Grachev, A. Hofstaetter, E. Kokanyan, A. Sharman, and O. Shirmer, Phys. Rev. B **65**, 224116 (2002).
[28] N. M. Pinhal and N. V. Vugman, J. Phys. C **18**, 6273 (1985).
[29] J. A. Aramburu, M. Moreno, K. Doclo, C. Daul, and M. T. Barriuso, J. Chem. Phys. **110**, 1497 (1999).
[30] M. T. Barriuso, J. A. Aramburu, and M. Moreno, J. Mol. Struct.: THEOCHEM **537**, 117 (2001).